Age-related changes in the ease of dynamical transitions in human brain activity

Takahiro Ezaki[1,2,3], Michiko Sakaki[4,5], Takamitsu Watanabe[6], Naoki Masuda[7,*]

[1]PRESTO, JST, 4-1-8 Honcho, Kawaguchi, Saitama, Japan

[2]National Institute of Informatics, Hitotsubashi, Chiyoda-ku, Tokyo, Japan

[3]Kawarabayashi Large Graph Project, ERARO, JST, c/o Global Research Center for Big Data Mathematics, NII, Chiyoda-ku, Tokyo, Japan

[4]School of Psychology and Clinical Language Sciences, University of Reading, Earley Gate, Whiteknights Road, Reading, United Kingdom

[5]Research Institute, Kochi University of Technology, Kami, Kochi, Japan.

[6]Institute of Cognitive Neuroscience, University College London, 17 Queen Square, London, WC1N 3AZ, United Kingdom

[7]Department of Engineering Mathematics, University of Bristol, Clifton, Bristol, United Kingdom

*** Corresponding Author:**

N. Masuda (naoki.masuda@bristol.ac.uk)

Department of Engineering Mathematics, University of Bristol, Clifton, Bristol, United Kingdom

Phone: +44-117-3315176

E-mail: naoki.masuda@bristol.ac.uk

Number of display items: 10 (8 figures and 2 tables)

Abbreviated title:

Age-related changes in brain activity

Competing financial interests

The authors declare no competing financial interests.

Acknowledgments

TE acknowledges the support provided through PRESTO, JST (No. JPMJPR16D2). MS acknowledges the support provided through the European Commission (PCIG13-GA-2013-618600) and the JSPS (16H05959; 16KT0002; 16H02053). TW acknowledges the support provided through the European Commission. NM acknowledges the support provided through CREST, JST (No. JPMJCR1304) and Kawarabayashi Large Graph Project, ERATO, JST (No. JPMJER1201).

Abstract

Executive functions, a set of cognitive processes that enable flexible behavioral control, are known to decay with aging. Because such complex mental functions are considered to rely on the dynamic coordination of functionally different neural systems, the age-related decline in executive functions should be underpinned by alteration of large-scale neural dynamics. However, the effects of age on brain dynamics have not been firmly formulated. Here, we investigate such age-related changes in brain dynamics by applying "energy landscape analysis" to publicly available functional magnetic resonance imaging data from healthy younger and older human adults. We quantified the ease of dynamical transitions between different major patterns of brain activity, and estimated it for the default mode network (DMN) and the cingulo-opercular network (CON) separately. We found that the two age groups shared qualitatively the same trajectories of brain dynamics in both the DMN and CON. However, in both of networks, the ease of transitions was significantly smaller in the older than the younger group. Moreover, the ease of transitions was associated with the performance in executive function tasks in a doubly dissociated manner: for the younger adults, the ability of executive functions was mainly correlated with the ease of transitions in the CON, whereas that for the older adults was specifically associated with the ease of transitions in the DMN. These results provide direct biological evidence for age-related changes in macroscopic brain dynamics and suggest that such neural dynamics play key roles when individuals carry out cognitively demanding tasks.

Introduction

Normal aging is associated with the decline in many mental functions which affects older adults' quality of life (Davis et al., 2010). While some cognitive skills (e.g., vocabulary and other crystalized knowledge about general information) are maintained with age, a clear age-related decline has been observed in executive functions which allow for flexible and goal-directed cognitive control by integrating diverse information (Park et al., 2002; Salthouse, 2009). Given accumulating evidence for associations between efficient integration of cognitive information and finely-coordinated large-scale neural dynamics (Fries, 2005; Rolls et al., 2008; Deco et al., 2011; Uhlhaas and Singer, 2012; Kopell et al., 2014; Wang and Krystal, 2014; Watanabe and Rees, 2017), it is reasonable to assume that such age-related deterioration of executive functions is underpinned by age-associated changes in neural dynamics.

Theoretically, some studies have suggested crucial roles of brain dynamics in age-related alterations of executive functions (Nakagawa et al., 2013; Rolls and Deco, 2015). Behavioral research also suggests that cognitive decline with aging is relevant to dynamics – in particular transitory dynamics (i.e., temporal transitions in behavioral states). For example, older adults, relative to younger adults, are more distracted by task-irrelevant information, such as their internal thoughts and external events (Hasher et al., 1991; Gazzaley et al., 2005). These results suggest that transitions from one state to another may happen too frequently in the older-aged brain as well as in older adults' behavior.

Empirically, however, whether and how declines in cognitive functions are correlated with age-related alterations in large-scale neural dynamics are poorly understood. Previous human neuroimaging studies have reported associations between age-related cognitive changes and static brain architecture, such as focal white/gray matter structures (Allen et al., 2005; Raz et al., 2005; Andrews-Hanna et al., 2007; Persson et al., 2016) and density of neurochemical substances (Berry et al., 2016). In addition, associations between age-related cognitive changes and dynamical features of the brain, such as functional connectivity (Andrews-Hanna et al., 2007; Damoiseaux et al., 2008; Esposito et al., 2008; Sambataro et al., 2010; Grady et al., 2010; Onoda et al., 2012; Tomasi and Volkow, 2012; Grady, 2012; Meier et al., 2012; Ferreira and Busatto, 2013; Geerligs et al., 2014, 2015; Madhyastha and Grabowski, 2014), signal variability (Garrett et al., 2010, 2013), 1/*f* noise (Voytek et al., 2015), patterns of brain activity during tasks (Davis et al., 2008; Jimura and Braver,

2010), and neural oscillations (Pons et al., 2010; Voytek and Knight, 2015) have been investigated. However, these studies neither revealed how different parts of the brain dynamically integrate and disintegrate to create different activity patterns nor how one's brain transits among different activity patterns.

To address this fundamental question on aging brains, here, we conceptualized "ease of transitions" in neural dynamics as the rate of transitions between different major brain activity patterns that frequently appear during rest. We tested (i) whether the ease of transitions in neural dynamics is different between older versus younger adults, and (ii) whether the association between the executive ability and the ease of transitions in neural dynamics differs between younger and older adults. To address these questions, we focused on the default mode network (DMN) (Raichle et al., 2001) and the cingulo-opercular network (CON) (Dosenbach et al., 2007). We chose the DMN and CON for two reasons. First, recent studies suggested that the executive ability of older adults depends more strongly on the DMN than that of younger adults (Duverne et al., 2009; Turner and Spreng, 2015; Maillet and Schacter, 2016). Second, the CON is implicated in executive functions in older adults (Meier et al., 2012; Amer et al., 2016; Schmidt et al., 2016).

We characterized neural dynamics of the DMN and CON by applying a data-driven approach called energy landscape analysis (Watanabe et al., 2014a, 2014b; Ezaki et al., 2017; Watanabe and Rees, 2017) to resting-state functional MRI (fMRI) signals collected from younger (18yo ≤ and ≤ 30yo) and older adults (60yo ≤ and ≤ 85yo) (Table 1). Our analysis pipeline is schematically shown in Fig. 1. Technically, for each brain system (Fig. 2), we first inferred an energy landscape and then estimated neural dynamics as movements of a "ball" on the landscape (Fig. 3). Activity patterns with a small energy value (i.e., lower positions on the landscape) appear with a high frequency. Based on the neural dynamics, we identified major brain activity patterns as those frequently visited and located at the bottom of a basin in the energy landscape, and finally quantified the ease of dynamical transitions based on the frequency with which major activity patterns were visited. Because the fronto-parietal network (FPN) has also been implicated in aging of executive functions (Dosenbach et al., 2008), we additionally carried out the analysis on FPN but did not obtain significant results. We will discuss this point in Discussion.

Materials and Methods

Participants

We used data from 28 younger adults (19-30yo) and 28 older adults (60-85yo) from the Nathan Kline Institute's (NKI) Rockland phase I Sample (Table 1; Nooner et al., 2012): http://fcon_1000.projects.nitrc.org/indi/pro/nki.html. A similar age cut-off has been widely used in the literature on cognitive aging (Park et al., 2010b; Chadick et al., 2014). The two groups were matched on race and sex, and did not significantly differ in IQ (Table 1). All of them were right handed. Data from one younger female participant were not included in the analyses of behavioral scores because she did not complete a cognitive task.

Behavioral data and executive score

Participants' executive functions were assessed by the Delis-Kaplan Executive Function System (D-KEFS) (Delis et al., 2001, 2004) which consists of multiple cognitive tests to assess executive functions. In accordance with previous literature (Latzman and Markon, 2010; Barbey et al., 2012), we constructed a composite executive score for each individual by applying a factor analysis to scores from five tests in D-KEFS (Table S1): verbal fluency, sorting task, 20 questions, color word task, and design fluency. The analysis revealed three factors with the eigenvalues greater than 1 but the scree plot showed only one sharp bend in the array to eigenvalues after the first factor. Therefore, the factor score for the first factor was used as an executive score in the current study. The eigenvalue of this factor was 4.26 and it accounted for 43% of the variance with all items having positive loadings (Table S1). Participants' IQ was assessed by the Wechsler Abbreviated Scale of Intelligence (WASI) (Wechsler, 1999); a full scale intelligence quotient, verbal IQ, and performance IQ scores were used in the current study.

Definition of brain systems

We determined the regions of interest (ROIs) of the DMN and CON by employing the coordinates obtained in a previous study (Fair et al., 2009). The original systems have 12 and 7 ROIs for the DMN and CON, respectively (Fig. 2). For the DMN, the pairwise maximum entropy model (MEM) did not yield a high accuracy of fit, presumably due to the insufficiency in the data length (Table 2). It should be noted that in the

pairwise MEM, the accuracy of fit generally decreases with N_{ROI} if the amount of the observed data is fixed (Ezaki et al., 2017; Watanabe et al., 2013). Therefore, we analyzed the right- and left-hemisphere DMNs (the right/left DMN with 8 ROIs, respectively) instead of the original DMN. The number of ROIs for these one-hemisphere systems was not equal to the half of the original DMN because some ROIs (i.e., amPFC, vmPFC, pCC, and retro splen) were almost on the midline such that they were used in both the right and left DMNs.

fMRI data acquisition and preprocessing

The MRI data were recorded in a 3T scanner (MAGNETOM, TrioTim syngo MR B15, Siemens). fMRI data were obtained during rest with an echo planner imaging (EPI) sequence (TR = 2500ms, TE = 30ms, flip angle = 80°, 38 slices, spatial resolution = $3\times3\times3mm^3$, FOV = 216ms, acquisition time = 10m 55s). Anatomical images were acquired with T1-weighted sequence (MPRAGE) (TR = 2500ms, TE = 3.5ms, flip angle = 8°, spatial resolution = $1\times1\times1mm^3$). During the EPI data acquisition, the participants were asked to be relaxed with their eyes open.

Data preprocessing was performed using FMRIB's Software Library (FSL; www.fmrib.ox.ac.uk/fsl), including skull stripping of structural images with BET, motion correction with MCFLIRT, and smoothing with full-width half-maximum 5 mm. Registration was performed with FLIRT; each functional image was registered to the participant's high-resolution brain-extracted structural image and the standard Montreal Neurological Institute (MNI) 2-mm brain. We also applied additional preprocessing steps to the functional data to remove spurious variance. First, we regressed out six head motion parameters, global signal, cerebrospinal fluid (CSF) signal, and white matter (WM) signal with FSL FEAT. For each participant, CSF, gray matter (GM) and WM were segmented through FSL's FAST based on his/her T1. We next applied band-pass temporal filtering (0.01-0.1 Hz). The data were then re-smoothed by Gaussian kernels with sigma = 2.12 (the same setting as the one applied during the initial smoothing) with an FSL command line tool called SUSAN to improve the signal-to-noise ratio. Finally, we extracted the global signal for each volume again and subtracted this global signal from the averaged signal of all voxels within each spherical ROI (radius = 4mm) in the DMN and CON (Watanabe et al., 2013, 2014b). In this way, we avoided overestimation of synchronization in brain activity between different ROIs.

We confirmed that the magnitude of the head motion was not significantly different between the younger and older adults ($t_{54} = -0.33$, $P = 0.75$). We quantified the magnitude of the head motion by the average displacement of each volume relative to the previous volume, computed from the translation parameters in the *x* (left/right), *y* (anterior/posterior), and *z* (superior/inferior) directions as $\sqrt{x^2 + y^2 + z^2}$ (Van Dijk et al., 2012).

Fitting of the pairwise MEM

We fitted the pairwise MEM to the fMRI data using a standard method as follows (Ezaki et al., 2017; Watanabe et al., 2013; Fig. 1). Because the method demands a relatively large amount of data, we pooled the fMRI signals from the participants in the same age group and then fitted a pairwise MEM. Consider a system of N_{ROI} ROIs. For each ROI, labeled i (=1, … , N_{ROI}), we denote the binarized activity at time t by σ_i^t ($1 \leq t \leq T$), which is equal to either +1 (active) or –1 (inactive). For each ROI in each participant, we set a threshold, above which we regarded the ROI to be active, to the average signal value for the ROI across time for the participant, resulting in approximately 50% of time points being active for the ROI for the participant. Thus, the threshold value was different across ROIs and across participants. We confirmed that the accuracy of fitting, defined in the following, is insensitive to the threshold value as long as the fraction of active time points falls within 0.25 and 0.75 (Fig. S1). The activity pattern at time t is specified by an N_{ROI}-dimensional binary vector $[\sigma_1^t, \sigma_2^t, \ldots, \sigma_{N_{\mathrm{ROI}}}^t]$ (Fig. 3). Note that there are $2^{N_{\mathrm{ROI}}}$ possible activity patterns, which are enumerated as $V_1 = [-1, -1, \ldots, -1]$, …, $V_{2^{N_{\mathrm{ROI}}}} = [1, 1, \ldots, 1]$.

For each ROI, we aggregated the data over time and across the participants in the same age group, and calculated the frequency that each activity pattern V_k ($k = 1, \ldots, 2^{N_{\mathrm{ROI}}}$) was realized, denoted by $P_{\mathrm{empirical}}(V_k)$. For the pairwise MEM, the frequency obeys the Boltzmann distribution,

$$P(V_k) = e^{-E(V_k)} / \sum_{l=1}^{2^{N_{\mathrm{ROI}}}} e^{-E(V_l)}, \qquad \text{[Eq. 1]}$$

where $E(V_k)$ represents the energy for activity pattern V_k defined by

$$E(V_k) = -\sum_{i=1}^{N} h_i \sigma_i - (1/2) \sum_{i=1}^{N_{\mathrm{ROI}}} \sum_{j=1}^{N_{\mathrm{ROI}}} J_{ij} \sigma_i \sigma_j. \qquad \text{[Eq. 2]}$$

Here, the fitting parameters h_i and J_{ij} represent the tendency for the *i*th ROI to be active when it is isolated and the strength of the interaction between the *i*th and *j*th ROIs, respectively. A small energy value corresponds to a large frequency of appearance of an activity pattern by definition.

To obtain h_i and J_{ij} (i, j = 1, ..., N_{ROI}), we first calculated the average and pairwise correlation of the empirical data as follows:

$$\langle \sigma_i \rangle = (1/T) \sum_{t=1}^{T} \sigma_i^t, \quad \text{[Eq. 3]}$$

$$\langle \sigma_i \sigma_j \rangle = (1/T) \sum_{t=1}^{T} \sigma_i^t \sigma_j^t. \quad \text{[Eq. 4]}$$

The average and correlation expected from the model [Eq. 1] for given h_i and J_{ij} (i, j = 1, ..., N) are equal to $\langle \sigma_i \rangle_{\mathrm{m}} = \sum_{k=1}^{2^{N_{\mathrm{ROI}}}} \sigma_i(V_k) P(V_k)$ and $\langle \sigma_i \sigma_j \rangle_{\mathrm{m}} = \sum_{k=1}^{2^{N_{\mathrm{ROI}}}} \sigma_i(V_k) \sigma_j(V_k) P(V_k)$, respectively. We iteratively adjusted h_i and J_{ij} according to $h_i^{\mathrm{new}} = h_i^{\mathrm{old}} + \alpha(\langle \sigma_i \rangle - \langle \sigma_i \rangle_{\mathrm{m}})$ and $J_{ij}^{\mathrm{new}} = J_{ij}^{\mathrm{old}} + \alpha\big(\langle \sigma_i \sigma_j \rangle - \langle \sigma_i \sigma_j \rangle_{\mathrm{m}}\big)$ such that the values of $\langle \sigma_i \rangle_{\mathrm{m}}$ and $\langle \sigma_i \sigma_j \rangle_{\mathrm{m}}$ gradually approach the empirical values [Eqs. 3 and 4]. This iterative scheme is a gradient decent method minimizing the Kullback-Leibler divergence given by $D_2 = \sum_{k=1}^{2^{N_{\mathrm{ROI}}}} P_{\mathrm{empirical}}(V_k) \cdot \log_2(P_{\mathrm{empirical}}(V_k)/P_{\mathrm{model}}(V_k))$. We set $\alpha = 0.1$.

Accuracy of fit

We used the following accuracy measure (Schneidman et al., 2006; Shlens et al., 2006; Watanabe et al., 2013, 2014a, 2014b; Ezaki et al., 2017) to assess the goodness of the fit of the pairwise MEM to the fMRI data obtained from each age group:

$$r_D = (D_1 - D_2)/D_1, \quad \text{[Eq. 5]}$$

where D_1 represents the Kullback-Leibler divergence between the MEM and data when the MEM is restricted to have no interaction term, i.e., $J_{ij} = 0$ for all *i* and *j*. We obtain $r_D = 1$ when the pairwise MEM perfectly reproduces the empirical distribution of activity patterns, whereas $r_D = 0$ when the pairwise interaction (i.e., J_{ij}) does not contribute to improve the fitting.

Disconnectivity graph

For each age group, we calculated a disconnectivity graph (Becker and Karplus, 1997; Wales et al., 1998; Wales, 2010) from the estimated pairwise MEM in the same way as was done in our previous studies (Watanabe et al., 2014a, 2014b; Watanabe and Rees, 2017). In the network of activity patterns, where each activity pattern constitutes a node, activity patterns V_k and $V_{k'}$ were defined to be adjacent (i.e., directly connected by an edge) if they were the same across all ROIs except for one. Therefore, each activity pattern was adjacent to N activity patterns. For example, if $N_{\mathrm{ROI}} = 3$, activity pattern [1, 1, 1] is adjacent to [–1, 1, 1], [1, –1, 1], and [1, 1, –1]. Then, we identified the activity patterns whose energy values were smaller than all of their N_{ROI} adjacent activity patterns, i.e., local minimums in the energy landscape (bottom of a basin in Fig. 3). Local minimums are the activity patterns that are more likely to appear than all their neighboring patterns.

We obtained the disconnectivity graph from the network of activity patterns as follows. First, we identified all local minimums by exhaustively examining whether each activity pattern was a local minimum. Second, we set an energy threshold value, denoted by E_{th}, to the energy value of the activity pattern that attained the second largest energy value among the $2^{N_{\mathrm{ROI}}}$ activity patterns. Third, we removed the nodes corresponding to the activity patterns whose energy exceeded E_{th}. When E_{th}, is the second largest energy, the node with the largest energy was removed. We also removed the edges incident to the removed nodes. Fourth, we checked whether each pair of local minimums was connected in the reduced network. Fifth, we lowered E_{th} to the next largest energy value realized by an activity pattern. Then, we repeated the third to fifth steps, i.e., removal of the nodes and edges, checking of connectivity between local minimums, and lowering of E_{th}, until all the local minimums were isolated. In the course of the procedure, we obtained for each pair of local minimums the largest E_{th} value at which the two local minimums were disconnected. This E_{th} value is equal to the energy barrier that the dynamics of the brain have to overcome to reach from one local minimum to the other. Finally, we constructed a hierarchical tree whose terminal leaves represented the local minimums. The vertical positions of these leaves represent their energy values. Those of the branches represent the height of the energy barrier that separates the local minimums belonging to the two branches.

Attractive basin of a local minimum

The attractive basin of an energy local minimum for each age group was computed as follows (Stillinger and Weber, 1984; Becker and Karplus, 1997; Zhou, 2011; Watanabe et al., 2014a, 2014b; Ezaki et al. 2017; Watanabe and Rees, 2017). First, we selected a node i in the network of activity patterns. If the selected node was not a local minimum, we moved to the node with the smallest energy value among the nodes adjacent to the currently visited node. We repeated moving downhill in this manner until a local minimum was reached. The initial node i belongs to the basin of the finally reached local minimum. We ran this procedure for each initial node i.

Index of ease of dynamic transitions: Efficiency score

For each network, we denote the two synchronized activity patterns by $s_+ = [1, 1, \ldots, 1]$ (i.e., all ROIs are active) and $s_- = [-1, -1, \ldots, -1]$ (i.e., all ROIs are inactive). For each individual, we defined the rate of transitions between s_+ and s_- as the sum of the number of times that the activity $[\sigma_1^t, \sigma_2^t, \ldots, \sigma_{N_{\mathrm{ROI}}}^t]$ has left s_+ and arrived at s_- before revisiting s_+, and the number of times that $[\sigma_1^t, \sigma_2^t, \ldots, \sigma_{N_{\mathrm{ROI}}}^t]$ has left s_- and arrived at s_+ before revisiting s_-, divided by the number of volumes.

We denote by b_+ the attractive basin of s_+ excluding s_+ and by b_- the attractive basin of s_- excluding s_-. Because the disconnectivity graph of the DMN had only two major activity patterns, s_+ and s_- (Fig. 4A), we classified all activity patterns of the DMN into the following four categories: s_+, s_-, b_+, and b_- (Fig. 6A). Because the disconnectivity graph of the CON had a few local minimums in addition to s_+ and s_-, we classified the activity patterns of the CON into five categories: s_+, s_-, b_+, b_-, and the others (denoted by b_{other}) (Fig. 6B). To define the rate of peripheral transitions for each individual, we first calculated the rate of transitions between b_+ and b_- as the sum of the number of times that $[\sigma_1^t, \sigma_2^t, \ldots, \sigma_{N_{\mathrm{ROI}}}^t]$ for the individual transited from b_+ to b_- and the number of times that $[\sigma_1^t, \sigma_2^t, \ldots, \sigma_{N_{\mathrm{ROI}}}^t]$ transited from b_- to b_+, divided by the number of volumes. It should be noted that we used b_+ and b_- that were derived from the energy landscape calculated for the age group to which the focal individual belongs, whereas we counted the transitions between b_+ and b_- for the fMRI signals obtained from the individual, not the group of individuals. We refer to transitions between b_+ and b_- that do not involve transitions to s_+ or s_- as peripheral transitions. Precisely,

the rate of peripheral transitions was defined as the rate of transitions between b_+ and b_- subtracted by the rate of transitions between s_+ and s_-. The efficiency score for an individual was defined as the ratio of the rate of transitions between s_+ and s_- to the rate of peripheral transitions. Thus, the efficiency score reflects how frequently transitions between different major brain activity patterns occur relative to peripheral transitions.

Numerical simulations

We carried out numerical simulations to emulate brain dynamics constrained on the estimated energy landscape. As in our previous studies (Watanabe et al., 2014a, 2014b; Watanabe and Rees, 2017), we employed the Metropolis-Hastings algorithm (Chib and Greenberg, 1995; Zhou, 2011). First, we set the initial activity pattern to s_+. Then, in each time step, a transition from the current activity pattern V_k to one of its N adjacent activity patterns $V_{k'}$, selected with probability $1/N$, was attempted. The transition to the selected pattern took place with probability $p = \min[1, \exp\{E(V_k) - E(V_{k'})\}]$. With probability $1 - p$, the attempted transition was discarded. We ran the dynamics for sufficiently many time steps, i.e., 10^8, such that the initial condition did not influence the results.

Statistics

The age factor in our analysis of variance (ANOVA) was dichotomous (i.e., younger versus older). We made this choice because we had to pool data over participants in each age group to secure a sufficient amount of data for the present analysis.

In the analysis at the individual's level, we excluded outliers based on the Tukey's criteria of 1.5 interquartile range (Tukey, 1977). We confirmed that our main results were not affected by the choice of a method for excluding the effect of outliers (see *Supporting Information*).

Results

Behavioral results

General intelligence was not significantly different between younger and older individuals (performance IQ, $F_{1, 53} = 0.05$, $P = 0.83$; verbal IQ, $F_{1, 52} = 0.25$, $P = 0.25$; full IQ, $F_{1, 53} = 0.14$, $P = 0.71$) (Table 1). The older adults showed a significantly lower performance than the younger adults in terms of the executive score ($F_{1, 53} = 22.2$, $P < 0.001$, $\eta^2 = 0.22$) (Table 1). This result is consistent with the previous results on age-related declines in executive functions (Park et al., 2002; Salthouse, 2009) and suggests the validity of this behavioral index.

Accuracy of fitting of a pairwise MEM to fMRI data

We analyzed resting-state fMRI data from the younger and older individuals because such resting-state brain activity is considered to be closely related to various cognitive functions of humans (Deco et al., 2011). After pooling the binarized fMRI data across the participants in each age group (i.e., younger/older), we fitted the pairwise MEM for each age group and each system (i.e., DMN or CON) and found that in all the cases, the model accurately fitted to the empirical fMRI signals (accuracy of fit ≥ 83%, Table 2; Fig. 5A). In addition, the parameter values estimated for the pairwise MEM did not change when we estimated them for different subsets of the participants (Fig. 5B), suggesting the robustness of the current method. The accuracy of fit was consistently larger for the younger than older adults (Table 2), whose implication will be discussed in the Discussion section.

Identification of major activity patterns

Such accurate fitting of the pairwise MEM allows us to assign a hypothetical "energy value" to each of the $2^{N_{\mathrm{ROI}}}$ activity patterns. The energy value here is not a physical quantity but a computational construct rooted in statistical physics and uniquely encodes the probability with which each activity pattern appears (Fig. 3). By definition, an activity pattern with a smaller energy value occurs more frequently.

Based on the energy values assigned to all the $2^{N_{\mathrm{ROI}}}$ activity patterns, we built and analyzed an energy landscape for each brain system (i.e., DMN or CON) for each age group (Fig. 3) by creating a

disconnectivity graph for each energy landscape (Fig. 4). We refer to local minimums of the energy as major activity patterns. The disconnectivity graph shows the height of the barrier between an arbitrary pair of major activity patterns (the smallest height that one has to 'climb' to move from one major activity pattern to another).

For both the right and left DMNs in both age groups, the disconnectivity graph was composed of two local minimum activity patterns, which are s_+ (all ROIs are active) and s_- (all ROIs are inactive) (Fig. 4A). This result suggests that brain dynamics in the DMN are dominated by the synchronized activity patterns irrespectively of age.

Despite this similarity, the older group, relative to the younger group, had larger energy values (i.e., smaller frequency of appearance) at s_+ and s_- and a smaller energy barrier between s_+ and s_-, which suggests that dynamics of transitions between s_+ and s_- are different between the two groups. We corroborated this observation by carrying out an individual-level analysis to show that the frequency of visiting s_+ and s_- was significantly smaller for the older than younger adults ($t_{40} = 5.11$, $P_{\text{Bonferroni}} < 10^{-4}$, Cohen's $d = 1.36$) (the left panel of Fig. 4B).

In contrast, the CON had more complicated disconnectivity graphs with more branches and local minimums. Nevertheless, as was the same as the DMN, s_+ and s_- were the most major brain activity patterns with the smallest energies (i.e., the highest frequency of appearance) in both age groups (Fig. 4A), and they were visited with a higher frequency in the younger than the older group ($t_{44} = 4.03$, $P_{\text{Bonferroni}} < 10^{-3}$, $d = 1.08$) (the right panel of Fig. 4B).

Quantification of ease of transitions in brain dynamics

We hypothesized that the age-related differences in brain dynamics, or more specifically, ease of transitions (i.e., the rate of transitions between different major activity patterns), are linked to individuals' performance in executive functioning. To test this hypothesis, we used the inferred energy landscapes to quantify ease of transitions in the brain dynamics for each brain system and each age group. We then calculated frequencies of transitions between the four categories of activity patterns (DMN) or five categories (CON) for each

individual. We did so by directly investigating time series of the empirical data for each individual (Figs. 6B and 6C) and by performing random-walk numerical simulations for each age group to verify the validity of the present approach (Figs. 6D and 6E).

For the empirical fMRI data, we found that in both of the DMN and CON, the individuals in the younger group showed more frequent transitions between s_+ and s_- than those in the older group did ($F_{1,53} = 34.8$, $P < 10^{-6}$, $\eta^2 = 0.17$ for the main effect of Age in ANOVA [Age: younger/older] × [System: DMN/CON] on the rate of transitions between s_+ and s_-; Fig. 6B). In contrast, the individuals in the older group showed more frequent "peripheral transitions", i.e., transitions between b_+ and b_- that did not involve transitions to s_+ or s_- (see Materials and Methods for the definition) ($F_{1,53} = 25.1$, $P < 10^{-5}$, $\eta^2 = 0.06$ for the main effect of Age in another two-way factorial ANOVA [Age: younger/older] × [System: DMN/CON] on the peripheral transition score; Fig. 6C). In older adults, once their brain activity pattern exits from s_+ or s_-, the activity pattern tends to fluctuate between basins b_+ and b_- without easily reaching s_+ or s_- (Fig. 6F). The rank order of these results was reproduced by group-level numerical simulations of the random-walk model, which supports the validity of the present analysis method (Figs. 6D and 6E). Altogether, these results imply that brain dynamics of younger adults are more efficient than those of older adults in the sense of ease of transitions between s_+ or s_-.

We confirmed the implications of these results by quantifying the efficiency of brain dynamics for each individual using an "efficiency score". The efficiency score was defined as the ratio of the rate of transitions between s_+ and s_- to the rate of peripheral transitions. Four participants (one younger individual and three older individuals) were identified as outliers in terms of the efficiency score. After excluding these four participants, we found that the efficiency score was smaller in the older group than the younger group, in both DMN and CON (main effect of Age: $F_{1,49} = 21.6$, $P < 10^{-4}$, $\eta^2 = 0.12$ in a two-way factorial Age×System ANOVA; Fig. 7A). The same ANOVA also revealed a significant age-by-system interaction ($F_{1,49} = 4.53$, $P < 0.05$, $\eta^2 = 0.03$). This interaction reflects the fact that the difference in the efficiency score between the DMN and CON (DMN – CON) was significantly larger in the older group than the younger group ($t_{37} = 2.15$, $P < 0.05$, $d = 0.60$ in a post-hoc two-sample t-test), suggesting that compared to the CON, the ease of transitions in the DMN dynamics less deteriorates with aging.

354

355 **Association between efficiency of brain dynamics and executive ability**

356 Finally, we tested whether the efficiency score predicts the executive score. We found that the executive
357 score for the younger adults was significantly correlated with the efficiency score for the CON ($r = 0.57$, $P =$
358 0.0025, $P_{\text{Bonferroni}} < 0.05$, $df = 24$) but not with the efficiency score for the DMN ($r = –0.097$, $P = 0.64$, $df =$
359 24) (Fig. 7B). The older adults showed the opposite pattern: the executive score was not significantly
360 correlated with the efficiency score for the CON ($r = –0.099$, $P = 0.64$, $df = 23$), whereas it was significantly
361 correlated with the efficiency score for the DMN ($r = 0.54$, $P = 0.0057$, $P_{\text{Bonferroni}} < 0.05$, $df = 23$). These
362 results were robust against some variation in the threshold for binarizing fMRI signals, in particular in the
363 DMN (Fig. S4 in *Supporting Information*).

364

365 In addition, the correlation coefficient between the executive score and the efficiency score was significantly
366 larger for the DMN than the CON in the older group ($t_{22} = 2.20$, $P = 0.039$) but not in the younger group (t_{23}
367 $= –1.74$, $P = 0.096$) (Fig. 7C). It should be noted that the difference between the correlation coefficients was
368 assessed by the William's *t*-test for comparing two nonindependent correlations with a variable in common
369 (Weaver and Wuensch, 2013). Even after including the four outliers, the older adults still showed a stronger
370 correlation between their executive score and efficiency score for the DMN than for the CON ($t_{25} = 2.04$, $P =$
371 0.05), whereas the younger adults did not ($t_{25} = –0.26$, $P = 0.80$).

372

373 These results suggest that the executive ability of younger adults is related to the efficiency in brain
374 dynamics of the CON rather than that of the DMN, whereas the executive ability of older adults relies on the
375 DMN efficiency rather than on the CON efficiency. In contrast, the frequency of visiting the synchronized
376 activity patterns (i.e., s_+ or $s_–$), a simpler index to characterize large-scale dynamics in the brain, did not
377 consistently predict the executive score in the two age groups (DMN, younger: $r = 0.16$, $P = 0.41$, $df = 25$;
378 CON, younger: $r = 0.22$, $P = 0.26$, $df = 25$; DMN, older: $r = 0.38$, $P = 0.049$, $df = 26$; CON, older: $r = –0.014$,
379 $P = 0.47$, $df = 26$; all correlations, $P_{\text{Bonferroni}} > 0.05$).

380

381 **Association between functional connectivity and executive ability**

As a control analysis, we compared the within-system functional connectivity (FC) between the younger and older groups. The within-system FC was estimated as an averaged Pearson correlation over all pairs of ROIs belonging to each brain system (i.e., DMN or CON) The average of FC was calculated after applying Fisher's Z transformation to raw Pearson correlation values. In both DMN and CON, the within-network FC significantly declined with age (main effect of age group: $F_{1,53} = 36.2$, $P < 10^{-6}$, $\eta^2 = 0.23$ in a two-way factorial ANOVA, [Age: younger/older] × [System: DMN/CON]; Fig. 8). The interaction between the age and brain system was not significant ($F_{1,53} = 0.086$, $P = 0.77$). However, the FC was not significantly correlated with the executive score (DMN, younger: $r = 0.18$, $P = 0.37$, $df = 25$; CON, younger: $r = 0.27$, $P = 0.17$, $df = 25$; DMN, older: $r = 0.33$, $P = 0.085$, $df = 26$; CON, older: $r = 0.12$, $P = 0.53$, $df = 26$; uncorrected P values).

We also compared DMN-CON connectivity between the two age groups. The FC between the DMN and the CON was estimated as the Pearson correlation averaged over all pairs of ROIs one of which belongs to the DMN and the other to the CON. The DMN-CON FC declined with age ($t_{54} = 2.4$, $P = 0.019$, $d = 0.65$). This result is consistent with a previous study (Petrican et al., 2017). However, the DMN-CON FC was not significantly correlated with the executive score (younger: $r = 0.057$, $P = 0.78$, $df = 25$; older: $r = 0.13$, $P = 0.52$, $df = 26$).

Discussion

By applying the energy landscape analysis to resting-state fMRI data, we quantified "ease of transitions" in the intrinsic human brain dynamics and found its correlate with the executive functions of younger and older adults. While major activity patterns were similar between the different age groups, transitions between them were less frequent in the older than the younger adults, which was reflected in a significantly lower efficiency score of neural dynamics for the older adults. In particular, such a decline in the efficiency score due to aging was smaller at the DMN than the CON. In addition, we found that in the older adults, the efficiency score at the DMN, but not the CON, was correlated with their executive performance. By combining these findings, we suggest that brain dynamics in the DMN are critical to support older adults' executive functioning and that ease of transitions in neural dynamics may be essential for sustaining their executive performances.

DMN, CON, and other brain systems

We found that the ease of dynamical transitions observed in the CON's neural activity was correlated with the executive score in the younger but not older group. This result is consistent with previous observations suggesting critical roles of the CON in executive control (Dosenbach et al., 2007, 2008). In contrast, the ease of transitions in the DMN was correlated with the executive score in the older group specifically. These findings support the hypothesis that, differently from younger adults, older individuals heavily rely on the DMN rather than the CON for cognitive functions (Maillet and Schacter, 2016). A major support for this hypothesis has come from reduced deactivation within the DMN during cognitively demanding tasks, such as a difficult working memory task or semantic classification task (Maillet and Schacter, 2016). Our results for the DMN are consistent with this hypothesis.

We focused on the DMN and CON based on previous studies that predicted age-related changes in brain activity of the two brain systems (Maillet and Schacter, 2016). As a control, we analyzed an auditory network (Power et al., 2011), which should be less relevant to executive functioning and found no significant correlation between the efficiency and executive scores (see *Supporting Information*). These results suggest that the observed effects are specific to networks relevant to executive functioning.

Because the fronto-parietal network (FPN) has also been implicated in the effects of aging on executive functioning (Dosenbach et al., 2008), we also carried out the same set of analysis for the right-hemispheric and left-hemispheric FPNs but did not find the correlation between the executive score and the efficiency score (see *Supporting Information*). Such dissociated results between the CON and FPN may be due to their differential roles for higher-order cognitive functions. In fact, previous studies suggest that the CON and FPN have different time scales in top-down control (Dosenbach et al., 2008), are involved in different stages of working memory control (Wallis et al., 2015), and play dissociable roles in alertness (Sadaghiani and D'Esposito, 2015). Therefore, given that the current executive functioning score represents various cognitive components, future studies would have to compare neural dynamics of the CON and FPN using brain activity data during more specific psychological tasks.

Our energy landscape analysis method can treat only a relatively small number of ROIs. For this reason, we have not analyzed various other brain systems whose documented numbers of ROIs is large (Fair et al., 2009; Power et al., 2011). Furthermore, we have not analyzed inter-connected brain systems because the number of ROIs in such an inter-connected system is large. Yet aging is suggested to induce changes in structural and functional connectivity at a whole-brain level, either positive or negative, which may be related to modulation in information integration/channeling across modalities in aging (Andrews-Hanna et al., 2007; Allen et al., 2011; Meier et al., 2012; Chan et al., 2014; Geerligs et al., 2014; Spreng et al., 2016). Another consistently observed pattern is hemispheric asymmetry reduction in older adults (Cabeza, 2002). A large amount of data or a new technique is required to advance the applicability of the energy landscape analysis to combinations of brain systems as well as to a single brain system with a large number of ROIs. This is a main limitation of the current approach.

Energy landscape analysis and other methods for understanding brain dynamics

Signal variability analysis is a different data-driven approach to characterize brain dynamics. Prior research showed that fMRI signals were less variable over time for older than younger adults (Garrett et al., 2010, 2013). By referring to the phenomenon called the stochastic resonance, they speculated that a large amount of noise in fMRI signals observed for younger adults may be beneficial in efficient switching between energy local minimums corresponding to particular cognitive states. Although the present research did not

aim to test the stochastic resonance, our results are consistent with their theory in the point that dynamical transitions between the specified activity patterns, such as s_+ and s_-, are easier for younger than older adults. It should be noted that we explicitly constructed energy landscapes from fMRI data, whereas energy landscapes are conceptual objects in the previously conducted signal variability analysis.

In a separate line of research, a computational study employed simulations of biophysical models and suggests that the depth of the attractive basin in an energy landscape decreases by cognitive symptoms of schizophrenia, deteriorating short-term memory and attention (Loh et al., 2007). Our results are consistent with theirs, whereas participants' characteristics, methodologies, and relevant spatial scales are quite different between the two studies. Other computational approaches to aging used attractor dynamics and employed biophysical modelling as well (Nakagawa et al., 2013; Rolls and Deco, 2015). In contrast, in the current study, we revealed that the ease of transitions between the major activity patterns was different between the two age groups by analyzing large-scale brain dynamics in a data-driven manner without biophysical modeling.

We found that in both DMN and CON the within-network functional connectivity significantly declined with age, consistent with previous findings for the DMN (Andrews-Hanna et al., 2007; Damoiseaux et al., 2008; Esposito et al., 2008; Grady et al., 2010; Sambataro et al., 2010; Tomasi and Volkow, 2012; Onoda et al., 2012; Ferreira and Busatto, 2013; Geerligs et al., 2014, 2015; Madhyastha and Grabowski, 2014) and the CON (Meier et al., 2012; Geerligs et al., 2015). These connectivity results are consistent with our result that younger adults have shown larger synchronization than older adults in both DMN and CON (Fig. 4B). However, the functional connectivity in either DMN or CON was not correlated with the executive score. In addition, the functional connectivity in the DMN increased with age in some studies or did not change with age in other studies (Biswal et al., 2010; Koch et al., 2010; Park et al., 2010a; Allen et al., 2011; Jones et al., 2011; Meier et al., 2012; Campbell et al., 2013; Ferreira and Busatto, 2013; Persson et al., 2014; Ward et al., 2015; Turner and Spreng, 2015). Given these mixed results on age-related alterations in functional connectivity, the energy landscape analysis may provide an alternative promising approach towards understanding cognitive aging in the brain. We explicitly showed that as individuals age, transitions between

the synchronized activity patterns are reduced. Changes in functional connectivity alone do not tell how the ease of transitions is affected.

However, the energy landscape analysis is not the only method for revealing association between brain dynamics and cognitive aging. For example, parameter values estimated for a dynamic causal model were associated with cognitive performance, and the association was stronger for older than younger adults in a couple of brain systems including the DMN (Tsvetanov et al., 2016). This result is consistent with ours. Other methods that aim to minimize confounding effects of non-neuronal signals contained in fMRI signals may also yield similar results.

Dynamic functional connectivity is another method to track neural dynamics, in particular in fMRI data. As the name suggests, it analyzes time-varying correlation between pairs of ROIs using sliding windows or other methods (Hindriks et al., 2016; Choe et al., 2017). In contrast, energy landscape analysis quantifies changes of a collection of fMRI signals at different ROIs over time. At each time point, the brain state in the energy landscape analysis is given by a vector summarizing whether each ROI is active or inactive, rather than connectivity between ROIs. Investigating differences between the results produced by these two methods warrants future work.

Age-related changes in the brain

While we focused on younger and older adults in the paper, we carried out the same analysis using middle-aged individuals. The results were roughly in the middle between those for the younger group and those for the older group (Fig. S5). In accordance, the strength of the correlation between the efficiency and executive scores was not different between the DMN and the CON.

Age-related differences exist not only in neural activity. For example, aging is typically accompanied with the changes in the gray matter volume (e.g., Allen et al., 2005; Fjell et al., 2013). However, we confirmed that our results were not confounded by the gray matter volume (*Supporting Information*). In addition, older adults tend to show reduced heart rate variability, which in turn can lead to larger variances and noise in the functional connectivity of the resting-state BOLD signal (Tsvetanov et al., 2015). BOLD signals can also

include vascular/respiration signals that may differ between younger and older adults (Power et al., 2017). We were not able to assess the contribution of these factors to the present results due to the lack of the physiological data.

While the current sample showed age-related declines in executive functions as observed in the previous studies (Park et al., 2002; Salthouse, 2009), the IQ scores were not significantly different between younger and older adults in the present study unlike some previous studies (Kaufman et al., 1989). In a related vein, we did not find age-related changes in the head movement, while previous studies often reported that older adults would move more (Mowinckel et al., 2012). These results raise a question about the generalizability of the current findings. Future research should address whether similar patterns are obtained for other independent and larger samples.

Methodological issues

Our analysis method implicitly assumes that the brain dynamics are completely described by the shape of the energy landscape except for stochasticity. In particular, the history of brain dynamics is assumed not to influence the next activity pattern, whereas the current activity pattern can. Such a memoryless process is called a Markov process. With a discrete time step of TR = 2500ms, we validated the Markovian assumption by simulating Markovian random-walk processes whose transition probabilities were determined by the energy landscape. We found that numerically obtained transition rates (Figs. 6D and 6E) were close to those obtained directly from the empirical data (Figs. 6B and 6C) in both of the DMN and CON. The hidden Markov model is another approach that quantifies memoryless stochastic transitions between states and has been recently applied to neuroimaging data (Baker et al. 2014; Vidaurre et al. 2016). Comparison between such an approach and the present one warrants future work.

We did not look into the shape of disconnectivity graphs, which was different between the DMN and CON (Fig. 4A). The biological reason and functional relevance of this difference are unclear. Disconnectivity graphs of the DMN and CON during tasks may provide information regarding functional relevance of different attractive basins, as in our previous study using a bistable visual perception task (Watanabe et al., 2014b).

The maximum entropy model fitted better to the data obtained from the younger than older adults (Table 2). This was also the case for the FPN and the auditory network (*Supporting Information*). There are two possible reasons underlying this result. First, the younger group yielded a higher frequency of visit to the two synchronized activity patterns, which were by far the most frequently visited activity patterns. By definition, the value of the accuracy of fit would be large when the maximum entropy model accurately estimates the frequency of visit to frequent activity patterns, even if the model is somewhat inaccurate on other activity patterns. A second possible reason is that we had to pool data across individuals in the same group and heterogeneity across the individuals may be larger for the older than the younger group. In the group-based analysis, the dependency of the accuracy of fit on the age may act as a covariate of no interest influencing the statistical results, which is a limitation of the present study. A larger amount of data to secure a high accuracy value for both groups or development of methods requiring less data will probably mitigate the problem.

The main results here were based on a set of ROIs defined in a previous study (Fair et al., 2009), whereas the supplementary results regarding the auditory network used a different and more detailed ROI set (Power et al., 2011). We did not use the finer atlas for DMN and CON (Power et al., 2011) because our method is limited to a relatively small number of ROIs (i.e., around 10 ROIs) given the current amount of data, but the DMN and CON in the finer atlas are composed of 59 and 14 ROIs, respectively. Even if we focus on a single brain hemisphere, the number of ROIs is still too large for our analysis. Furthermore, we should note that whichever brain atlas we use, the ROI coordinates are calculated based on neuroimaging data obtained from young adults. Therefore, the ROI coordinates used in the present study may underrepresent the brain of older adults (Geerligs et al. 2017). To address this concern, we conducted a seed-based functional connectivity analysis. We used a 4-mm sphere ROI in the right anterior insula [$x = 36$, $y = 16$, $z = 5$] as a seed for the CON (Sadaghiani and D'Esposito, 2015) and found that this seed region showed significant connectivity with most of the coordinates used to define the CON in the present study not only in younger adults but also in older adults (see Fig. S8 and Table S2). We also used a 4-mm sphere ROI in the posterior cingulate [$x = –2$, $y = –29$, $z = 39$] as a seed for the DMN. Once again, we found spatial maps that were similar between the two age groups and included most of the coordinates for the DMN for both age groups. The results were

573 qualitatively the same for the FPN, where the seed region was a 4-mm sphere ROI in the right dorsolateral
574 prefrontal cortex [$x = 43$, $y = 21$, $z = 38$]. These results suggest that, although the ROIs used in the current
575 study were defined based on a younger sample in a previous research (Fair et al. 2009), these ROIs are still
576 valid for both younger and older groups in our sample.
577
578 We removed the global signal before submitting the fMRI data to our analysis pipeline. However,
579 justification of global signal regression remains controversial. Global signal regression should be used with
580 care when one compares groups with different characteristics of fMRI signal fluctuations (Murphy and Fox,
581 2017), which may apply to the present study in which we compared younger and older groups. We opted not
582 to try different preprocessing methods because there is no gold standard and it is even difficult to select an
583 alternative preprocessing method (Murphy and Fox, 2017).
584
585 Our results indicate that resting-state data bring us useful information on cognitive aging. However,
586 integrating resting-state data with data during more specific cognitive tasks will further our understanding of
587 neural mechanisms underlying age-related cognitive decline (Campbell and Schacter, 2017; Geerligs and
588 Tsvetanov, 2017; Grady, 2017).

589 **References**

590 Allen EA et al. (2011) A baseline for the multivariate comparison of resting-state networks. Front Syst
591 Neurosci 5:2.

592 Allen JS, Bruss J, Brown CK, Damasio H (2005) Normal neuroanatomical variation due to age: The major
593 lobes and a parcellation of the temporal region. Neurobiol Aging 26:1245–1260.

594 Amer T, Anderson JAE, Campbell KL, Hasher L, Grady CL (2016) Age differences in the neural correlates
595 of distraction regulation: A network interaction approach. Neuroimage 139:231–239.

596 Andrews-Hanna JR, Snyder AZ, Vincent JL, Lustig C, Head D, Raichle ME, Buckner RL (2007) Disruption
597 of large-scale brain systems in advanced aging. Neuron 56:924–935.

598 Baker AP, Brookes MJ, Rezek IA, Smith SM, Behrens T, Probert Smith PJ, Woolrich M (2014) Fast
599 transient networks in spontaneous human brain activity. eLife 3:e01867.

600 Barbey AK, Colom R, Solomon J, Krueger F, Forbes C, Grafman J (2012) An integrative architecture for
601 general intelligence and executive function revealed by lesion mapping. Brain 135:1154–1164.

602 Becker OM, Karplus M (1997) The topology of multidimensional potential energy surfaces: Theory and
603 application to peptide structure and kinetics. J Chem Phys 106:1495–1517.

604 Berry AS, Shah VD, Baker SL, Vogel JW, O'Neil JP, Janabi M, Schwimmer HD, Marks SM, Jagust WJ
605 (2016) Aging affects dopaminergic neural mechanisms of cognitive flexibility. J Neurosci 36:12559–
606 12569.

607 Biswal BB et al. (2010) Toward discovery science of human brain function. Proc Natl Acad Sci 107:4734–
608 4739.

609 Cabeza R (2002) Hemispheric asymmetry reduction in older adults: The HAROLD model. Psychol Aging
610 17:85–100.

611 Campbell KL, Grigg O, Saverino C, Churchill N, Grady CL (2013) Age differences in the intrinsic
612 functional connectivity of default network subsystems. Front Aging Neurosci 5:73.

613 Campbell KL, Schacter DL (2017) Ageing and the resting state: is cognition obsolete? Lang Cogn Neurosci
614 32:661–668.

615 Chadick JZ, Zanto TP, Gazzaley A (2014) Structural and functional differences in medial prefrontal cortex
616 underlie distractibility and suppression deficits in ageing. Nat Commun 5:4223.

617 Chan MY, Park DC, Savalia NK, Petersen SE, Wig GS (2014) Decreased segregation of brain systems
618 across the healthy adult lifespan. Proc Natl Acad Sci 111:E4997–E5006.
619 Chib S, Greenberg E (1995) Understanding the Metropolis-Hastings algorithm. Am Stat 49:327–335.
620 Choe AS, Nebel MB, Barber AD, Cohen JR, Xu Y, Pekar JJ, Caffo B, Lindquist MA (2017) Comparing test-
621 retest reliability of dynamic functional connectivity methods. Neuroimage 158:155–175.
622 Damoiseaux JS, Beckmann CF, Sanz Arigita EJ, Barkhof F, Scheltens P, Stam CJ, Smith SM, Rombouts
623 SARB (2008) Reduced resting-state brain activity in the "default network" in normal aging. Cereb
624 Cortex 18:1856–1864.
625 Davis JC, Marra CA, Najafzadeh M, Liu-Ambrose T (2010) The independent contribution of executive
626 functions to health related quality of life in older women. BMC Geriatr 10:16.
627 Davis SW, Dennis NA, Daselaar SM, Fleck MS, Cabeza R (2008) Qué PASA? The posterior-anterior shift in
628 aging. Cereb Cortex 18:1201–1209.
629 Deco G, Jirsa VK, McIntosh AR (2011) Emerging concepts for the dynamical organization of resting-state
630 activity in the brain. Nat Rev Neurosci 12:43–56.
631 Delis DC, Kaplan E, Kramer JH (2001) Delis-Kaplan executive function system (D-KEFS). San Antonio:
632 Psychological Corporation.
633 Delis DC, Kramer JH, Kaplan E, Holdnack J (2004) Reliability and validity of the Delis-Kaplan Executive
634 Function System: An update. J Int Neuropsychol Soc 10:301–303.
635 Dosenbach NUF, Fair DA, Cohen AL, Schlaggar BL, Petersen SE (2008) A dual-networks architecture of
636 top-down control. Trends Cogn Sci 12:99–105.
637 Dosenbach NUF, Fair DA, Miezin FM, Cohen AL, Wenger KK, Dosenbach RAT, Fox MD, Snyder AZ,
638 Vincent JL, Raichle ME, Schlaggar BL, Petersen SE (2007) Distinct brain networks for adaptive and
639 stable task control in humans. Proc Natl Acad Sci 104:11073–11078.
640 Duverne S, Motamedinia S, Rugg MD (2009) The relationship between aging, performance, and the neural
641 correlates of successful memory encoding. Cereb Cortex 19:733–744.
642 Esposito F, Aragri A, Pesaresi I, Cirillo S, Tedeschi G, Marciano E, Goebel R, Di Salle F (2008)
643 Independent component model of the default-mode brain function: Combining individual-level and
644 population-level analyses in resting-state fMRI. Magn Reson Imaging 26:905–913.

Ezaki T, Watanabe T, Ohzeki M, Masuda N (2017) Energy landscape analysis of neuroimaging data. Phil Trans R Soc A 375:20160287.

Fair DA, Cohen AL, Power JD, Dosenbach NUF, Church JA, Miezin FM, Schlaggar BL, Petersen SE (2009) Functional brain networks develop from a "local to distributed" organization. PLoS Comput Biol 5:e1000381.

Ferreira LK, Busatto GF (2013) Resting-state functional connectivity in normal brain aging. Neurosci Biobehav Rev 37:384–400.

Fjell AM, et al. (2013). Critical ages in the life course of the adult brain: nonlinear subcortical aging. Neurobiol Aging 34:2239-2247.

Fries P (2005) A mechanism for cognitive dynamics: Neuronal communication through neuronal coherence. Trends Cogn Sci 9:474–480.

Garrett DD, Kovacevic N, McIntosh AR, Grady CL (2010) Blood oxygen level-dependent signal variability is more than just noise. J Neurosci 30:4914–4921.

Garrett DD, Samanez-Larkin GR, MacDonald SWS, Lindenberger U, McIntosh AR, Grady CL (2013) Moment-to-moment brain signal variability: a next frontier in human brain mapping? Neurosci Biobehav Rev 37:610–624.

Gazzaley A, Cooney JW, Rissman J, D'Esposito M (2005) Top-down suppression deficit underlies working memory impairment in normal aging. Nat Neurosci 8:1298–1300.

Geerligs L, Maurits NM, Renken RJ, Lorist MM (2014) Reduced specificity of functional connectivity in the aging brain during task performance. Hum Brain Mapp 35:319–330.

Geerligs L, Renken RJ, Saliasi E, Maurits NM, Lorist MM (2015) A brain-wide study of age-related changes in functional connectivity. Cereb Cortex 25:1987–1999.

Geerligs L, Tsvetanov KA (2017) The use of resting state data in an integrative approach to studying neurocognitive ageing—commentary on Campbell and Schacter (2016). Lang Cogn Neurosci 32:684–691.

Geerligs L, Tsvetanov KA, Cam-CAN, Henson RN (2017) Challenges in measuring individual differences in functional connectivity using fMRI: The case of healthy aging. Hum Brain Mapp 38:4125–4156.

Grady C (2012) The cognitive neuroscience of ageing. Nat Rev Neurosci 13:491–505.

673 Grady CL (2017) Cognition is never obsolete: a comment on Campbell and Schacter, 2016. Lang Cogn
674 Neurosci 32:681–683.
675 Grady CL, Protzner AB, Kovacevic N, Strother SC, Afshin-Pour B, Wojtowicz M, Anderson JAE, Churchill
676 N, McIntosh AR (2010) A multivariate analysis of age-related differences in default mode and task-
677 positive networks across multiple cognitive domains. Cereb Cortex 20:1432–1447.
678 Hasher L, Stoltzfus ER, Zacks RT, Rypma B (1991) Age and inhibition. J Exp Psychol Learn Mem Cogn
679 17:163–169.
680 Hindriks R, Adhikari MH, Murayama Y, Ganzetti M, Mantini D, Logothetis NK, Deco G (2016) Can
681 sliding-window correlations reveal dynamic functional connectivity in resting-state fMRI? Neuroimage
682 127:242–256.
683 Jimura K, Braver TS (2010) Age-related shifts in brain activity dynamics during task switching. Cereb
684 Cortex 20:1420–1431.
685 Jones DT, Machulda MM, Vemuri P, McDade EM, Zeng G, Senjem ML, Gunter JL, Przybelski SA, Avula
686 RT, Knopman DS, Boeve BF, Petersen RC, Jack CR (2011) Age-related changes in the default mode
687 network are more advanced in Alzheimer disease. Neurology 77:1524–1531.
688 Kaufman AS, Reynolds CR, McLean JE (1989) Age and WAIS-R intelligence in a national sample of adults
689 in the 20- to 74-year age range: A cross-sectional analysis with educational level controlled.
690 Intelligence 13:235–253.
691 Koch W, Teipel S, Mueller S, Buerger K, Bokde ALW, Hampel H, Coates U, Reiser M, Meindl T (2010)
692 Effects of aging on default mode network activity in resting state fMRI: Does the method of analysis
693 matter? Neuroimage 51:280–287.
694 Kopell NJ, Gritton HJ, Whittington MA, Kramer MA (2014) Beyond the connectome: The dynome. Neuron
695 83:1319–1328.
696 Latzman RD, Markon KE (2010) The factor structure and age-related factorial invariance of the Delis-
697 Kaplan Executive Function System (D-KEFS). Assessment 17:172–184.
698 Loh M, Rolls ET, Deco G (2007) A dynamical systems hypothesis of schizophrenia. PLoS Comput Biol
699 3:2255–2265.

700 Lövdén M, Li SC, Shing YL, Lindenberger U (2007) Within-person trial-to-trial variability precedes and
701 predicts cognitive decline in old and very old age: longitudinal data from the Berlin Aging Study.
702 Neuropsychologia 45:2827–2838.
703 MacDonald SWS, Li SC, Bäckman L (2009) Neural underpinnings of within-person variability in cognitive
704 functioning. Psychol Aging 24:792–808.
705 Madhyastha TM, Grabowski TJ (2014) Age-related differences in the dynamic architecture of intrinsic
706 networks. Brain Connect 4:231–241.
707 Maillet D, Schacter DL (2016) Default network and aging: Beyond the task-negative perspective. Trends
708 Cogn Sci 20:2014–2016.
709 Meier TB, Desphande AS, Vergun S, Nair VA, Song J, Biswal BB, Meyerand ME, Birn RM, Prabhakaran V
710 (2012) Support vector machine classification and characterization of age-related reorganization of
711 functional brain networks. Neuroimage 60:601–613.
712 Mowinckel AM, Espeseth T, Westlye LT (2012) Network-specific effects of age and in-scanner subject
713 motion: A resting-state fMRI study of 238 healthy adults. Neuroimage 63, 1364–1373.
714 Murphy K, Fox MD (2017) Towards a consensus regarding global signal regression for resting state
715 functional connectivity MRI. Neuroimage 154:169–173.
716 Nakagawa TT, Jirsa VK, Spiegler A, McIntosh AR, Deco G (2013) Bottom up modeling of the connectome:
717 Linking structure and function in the resting brain and their changes in aging. Neuroimage 80:318–329.
718 Nooner KB et al. (2012) The NKI-Rockland sample: A model for accelerating the pace of discovery science
719 in psychiatry. Front Neurosci 6:152.
720 Onoda K, Ishihara M, Yamaguchi S (2012) Decreased functional connectivity by aging is associated with
721 cognitive decline. J Cogn Neurosci 24:2186–2198.
722 Park DC, Lautenschlager G, Hedden T, Davidson NS, Smith AD, Smith PK (2002) Models of visuospatial
723 and verbal memory across the adult life span. Psychol Aging 17:299–320.
724 Park DC, Polk TA, Hebrank AC, Jenkins LJ (2010a) Age differences in default mode activity on easy and
725 difficult spatial judgment tasks. Front Hum Neurosci 3:75.
726 Park J, Carp J, Hebrank A, Park DC, Polk TA (2010b) Neural specificity predicts fluid processing ability in
727 older adults. J Neurosci 30:9253–9259.

728 Persson J, Pudas S, Nilsson L-G, Nyberg L (2014) Longitudinal assessment of default-mode brain function
729 in aging. Neurobiol Aging 35:2107–2117.
730 Persson N, Ghisletta P, Dahle CL, Bender AR, Yang Y, Yuan P, Daugherty AM, Raz N (2016) Regional
731 brain shrinkage and change in cognitive performance over two years: The bidirectional influences of
732 the brain and cognitive reserve factors. Neuroimage 126:15–26.
733 Petrican R, Taylor MJ, Grady CL (2017) Trajectories of brain system maturation from childhood to older
734 adulthood: Implications for lifespan cognitive functioning. Neuroimage 163:125–149.
735 Pons AJ, Cantero JL, Atienza M, Garcia-Ojalvo J (2010) Relating structural and functional anomalous
736 connectivity in the aging brain via neural mass modeling. Neuroimage 52:848–861.
737 Power JD, Cohen AL, Nelson SM, Wig GS, Barnes KA, Church JA, Vogel AC, Laumann TO, Miezin FM,
738 Schlaggar BL, Petersen SE (2011) Functional network organization of the human brain. Neuron
739 72:665–678.
740 Power JD, Plitt M, Laumann TO, Martin A (2017) Sources and implications of whole-brain fMRI signals in
741 humans. Neuroimage 146:609–625.
742 Raichle ME, MacLeod AM, Snyder AZ, Powers WJ, Gusnard DA, Shulman GL (2001) A default mode of
743 brain function. Proc Natl Acad Sci 98:676–682.
744 Raz N, Lindenberger U, Rodrigue KM, Kennedy KM, Head D, Williamson A, Dahle C, Gerstorf D, Acker
745 JD (2005) Regional brain changes in aging healthy adults: General trends, individual differences and
746 modifiers. Cereb Cortex 15:1676–1689.
747 Rolls ET, Deco G (2015) Stochastic cortical neurodynamics underlying the memory and cognitive changes
748 in aging. Neurobiol Learn Mem 118:150–161.
749 Rolls ET, Loh M, Deco G, Winterer G (2008) Computational models of schizophrenia and dopamine
750 modulation in the prefrontal cortex. Nat Rev Neurosci 9:696–709.
751 Sadaghiani S, D'Esposito M (2015) Functional characterization of the cingulo-opercular network in the
752 maintenance of tonic alertness. Cereb Cortex 25:2763–2773.
753 Salthouse TA (2009) Decomposing age correlations on neuropsychological and cognitive variables. J Int
754 Neuropsychol Soc 15:650–661.

Sambataro F, Murty VP, Callicott JH, Tan HY, Das S, Weinberger DR, Mattay VS (2010) Age-related alterations in default mode network: Impact on working memory performance. Neurobiol Aging 31:839–852.

Schmidt EL, Burge W, Visscher KM, Ross LA (2016) Cortical thickness in frontoparietal and cingulo-opercular networks predicts executive function performance in older adults. Neuropsychology 30:322–331.

Schneidman E, Berry MJ, Segev R, Bialek W (2006) Weak pairwise correlations imply strongly correlated network states in a neural population. Nature 440:1007–1012.

Shlens J, Field GD, Gauthier JL, Grivich MI, Petrusca D, Sher A, Litke AM, Chichilnisky EJ (2006) The structure of multi-neuron firing patterns in primate retina. J Neurosci 26:8254–8266.

Spreng RN, Stevens WD, Viviano JD, Schacter DL (2016) Attenuated anticorrelation between the default and dorsal attention networks with aging: evidence from task and rest. Neurobiol Aging 45:149–160.

Stillinger FH, Weber TA (1984) Packing structures and transitions in liquids and solids. Science 225:983–989.

Tomasi D, Volkow ND (2012) Aging and functional brain networks. Mol Psychiatry 17:549–558.

Tsvetanov KA, Henson RNA, Tyler LK, Davis SW, Shafto MA, Taylor JR, Williams N, Cam-CAN, Rowe JB (2015) The effect of ageing on fMRI: Correction for the confounding effects of vascular reactivity evaluated by joint fMRI and MEG in 335 adults. Hum Brain Mapp 36:2248–2269.

Tsvetanov KA, Henson RNA, Tyler LK, Razi A, Geerligs L, Ham TE, Rowe JB (2016) Extrinsic and intrinsic brain network connectivity maintains cognition across the lifespan despite accelerated decay of regional brain activation. J Neurosci 36:3115–3126.

Tukey JW (1977) Exploratory Data Analysis. Reading, Massachusetts: Addison-Wesley.

Turner GR, Spreng RN (2015) Prefrontal engagement and reduced default network suppression co-occur and are dynamically coupled in older adults: The default-executive coupling hypothesis of aging. J Cogn Neurosci 27:2462–2476.

Uhlhaas PJ, Singer W (2012) Neuronal dynamics and neuropsychiatric disorders: Toward a translational paradigm for dysfunctional large-scale networks. Neuron 75:963–980.

Van Dijk KRA, Sabuncu MR, Buckner RL (2012) The influence of head motion on intrinsic functional connectivity MRI. Neuroimage 59:431-438.

784 Vidaurre D, Quinn AJ, Baker AP, Dupret D, Tejero-Cantero A, Woolrich MW (2016) Spectrally resolved
785 fast transient brain states in electrophysiological data. Neuroimage 126:81-95.
786 Voytek B, Knight RT (2015) Dynamic network communication as a unifying neural basis for cognition,
787 development, aging, and disease. Biol Psychiatry 77:1089–1097.
788 Voytek B, Kramer MA, Case J, Lepage KQ, Tempesta ZR, Knight RT, Gazzaley A (2015) Age-related
789 changes in 1/f neural electrophysiological noise. J Neurosci 35:13257–13265.
790 Wales DJ (2010) Energy landscapes: Some new horizons. Curr Opin Struct Biol 20:3–10.
791 Wales DJ, Miller MA, Walsh TR (1998) Archetypal energy landscapes. Nature 394:758–760.
792 Wallis G, Stokes M, Cousijn H, Woolrich M, Nobre AC (2015) Frontoparietal and cingulo-opercular
793 networks play dissociable roles in control of working memory. J Cogn Neurosci 27:2019–2034.
794 Wang XJ, Krystal JH (2014) Computational psychiatry. Neuron 84:638–654.
795 Ward AM, Mormino EC, Huijbers W, Schultz AP, Hedden T, Sperling RA (2015) Relationships between
796 default-mode network connectivity, medial temporal lobe structure, and age-related memory deficits.
797 Neurobiol Aging 36:265–272.
798 Watanabe T, Hirose S, Wada H, Imai Y, Machida T, Shirouzu I, Konishi S, Miyashita Y, Masuda N (2013)
799 A pairwise maximum entropy model accurately describes resting-state human brain networks. Nat
800 Commun 4:1370.
801 Watanabe T, Hirose S, Wada H, Imai Y, Machida T, Shirouzu I, Konishi S, Miyashita Y, Masuda N (2014a)
802 Energy landscapes of resting-state brain networks. Front Neuroinform 8:12.
803 Watanabe T, Masuda N, Megumi F, Kanai R, Rees G (2014b) Energy landscape and dynamics of brain
804 activity during human bistable perception. Nat Commun 5:4765.
805 Watanabe T, Rees G (2017) Brain network dynamics in high-functioning individuals with autism. Nat
806 Commun 8:16048.
807 Weaver B, Wuensch KL (2013) SPSS and SAS programs for comparing Pearson correlations and OLS
808 regression coefficients. Behav Res 45:880-895.
809 Wechsler D (1999) Wechsler Abbreviated Scale of Intelligence. San Antonio: The Psychological
810 Corporation.
811 Zhou Q (2011) Random walk over basins of attraction to construct Ising energy landscapes. Phys Rev Lett
812 106:180602.

813

Figures and Tables

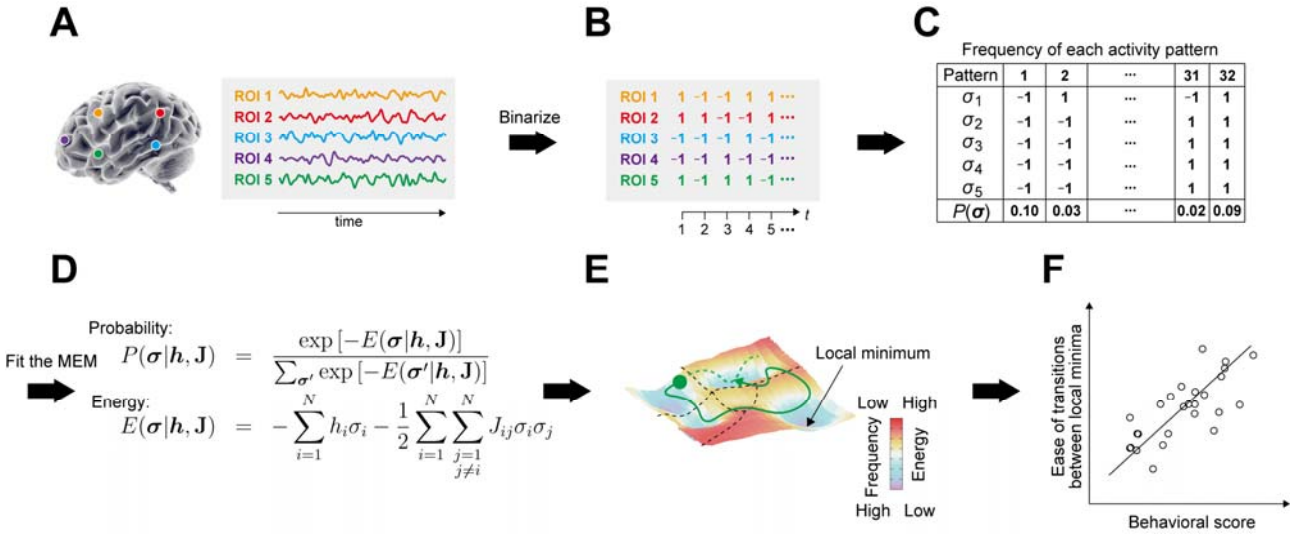

Figure 1. Pipeline of the energy landscape analysis. First, BOLD signals from selected ROIs (A) are binarized (B). Then, the frequency of each activity pattern is calculated (C). The distribution of the frequency of activity patterns is fitted by the MEM (D), from which an energy landscape is constructed (E). Finally, the brain dynamics quantified as the ease of transitions on the energy landscape (called "efficiency score") is associated with a participant's behavioral score (called "executive score").

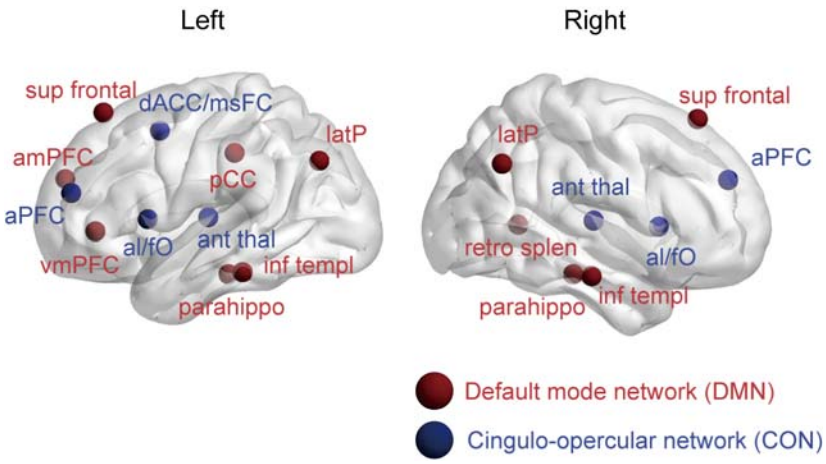

Figure 2. Location of the ROIs in each functional system. Retro splen: retro splenial cortex, latP: lateral parietal cortex, pCC: posterior cingulate cortex, parahippo: parahippocampal cortex, inf templ: inferior temporal cortex, sup frontal: superior frontal cortex, vmPFC: ventromedial prefrontal cortex, amPFC: anteromedial prefrontal cortex, ant thal: anterior thalamus, dACC/msFC: dorsal anterior cingulate cortex/medial superior frontal cortex, al/fO: anterior insula/frontal operculum, aPFC: anterior prefrontal cortex.

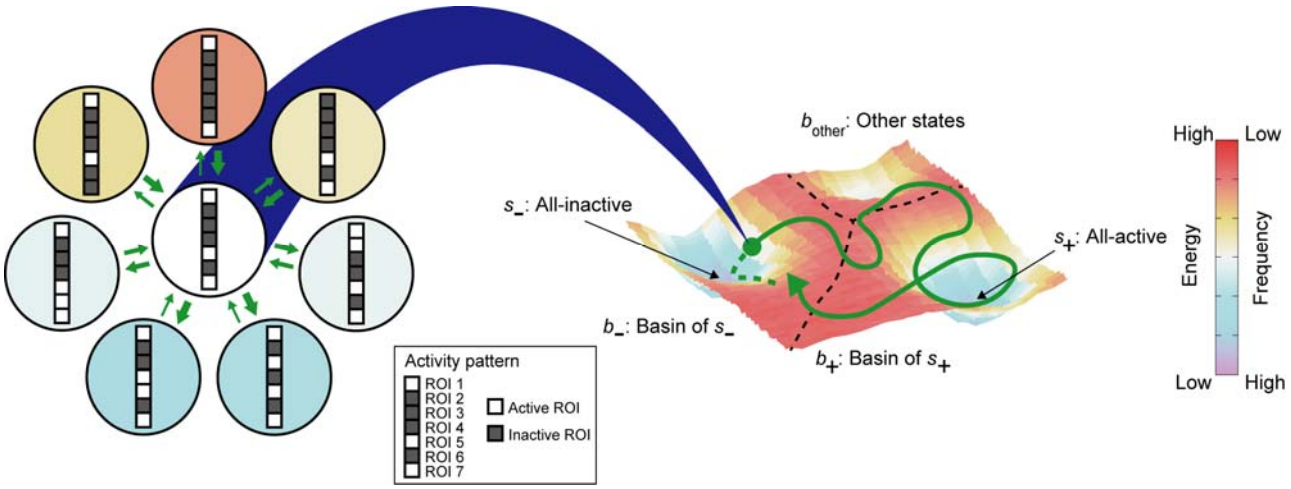

Figure 3. Schematic of dynamics of the activity pattern constrained on an energy landscape. The figure to the left is a blow-up of the figure to the right around an activity pattern. Because there are seven ROIs in this example, the focal activity pattern has seven neighboring activity patterns, as shown in the left figure. A transition to a neighboring activity pattern with a lower energy (shown in blue) is more likely to occur than a transition to an activity pattern with a higher energy (shown in a warm color).

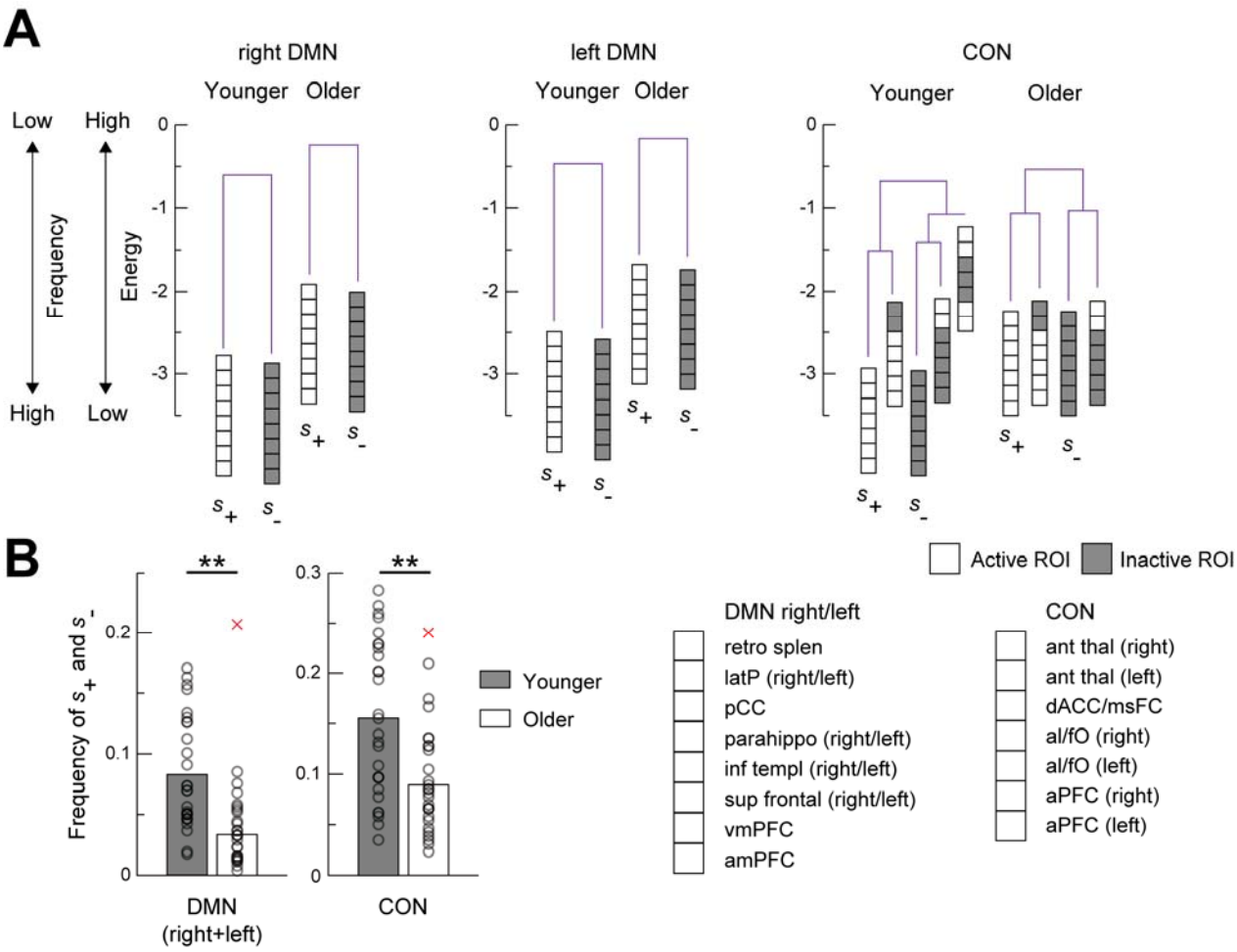

Figure 4. (A) Disconnectivity graph for each system and age group. (B) Frequency of s_+ and s_- for each system and age group. Each symbol and bar represent the results for a participant and their average, respectively. $^{**}P_{\text{Bonferroni}} < 0.01$, in two-sample t-tests ($N_{\text{younger}} = 28$ and $N_{\text{older}} = 27$). The crosses represent outliers. Note that inclusion of these outliers did not influence the statistical significance (DMN: $t_{53} = 3.76$, $P_{\text{Bonferroni}} < 10^{-3}$, $d = 1.01$, CON: $t_{49} = 3.39$, $P_{\text{Bonferroni}} < 0.01$, $d = 0.91$ in two-sample t-tests).

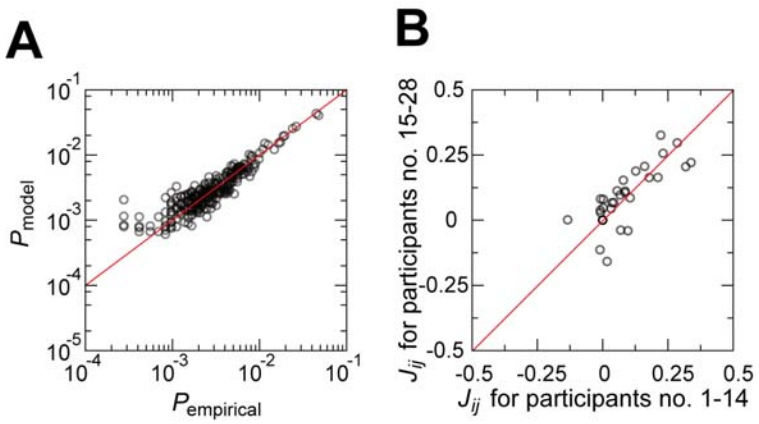

Figure 5. Fitting of the pairwise MEM. (A) Comparison between the probability with which each activity pattern is realized. A circle represents one of the $2^{N_{ROI}}$ activity patterns. The diagonal is shown by the solid line. $P_{empirical}$ and P_{model} represent the probability for the empirical data and that based on the MEM, respectively. (B) Consistency between the estimated parameter values across participants. The J_{ij} values estimated from the first half of the participants and those estimated from the second half of the participants are compared. A circle corresponds to the J_{ij} value calculated for a pair of i and j. Both panels were based on the data obtained from the right DMN ($N_{ROI} = 8$) of the younger participants' group.

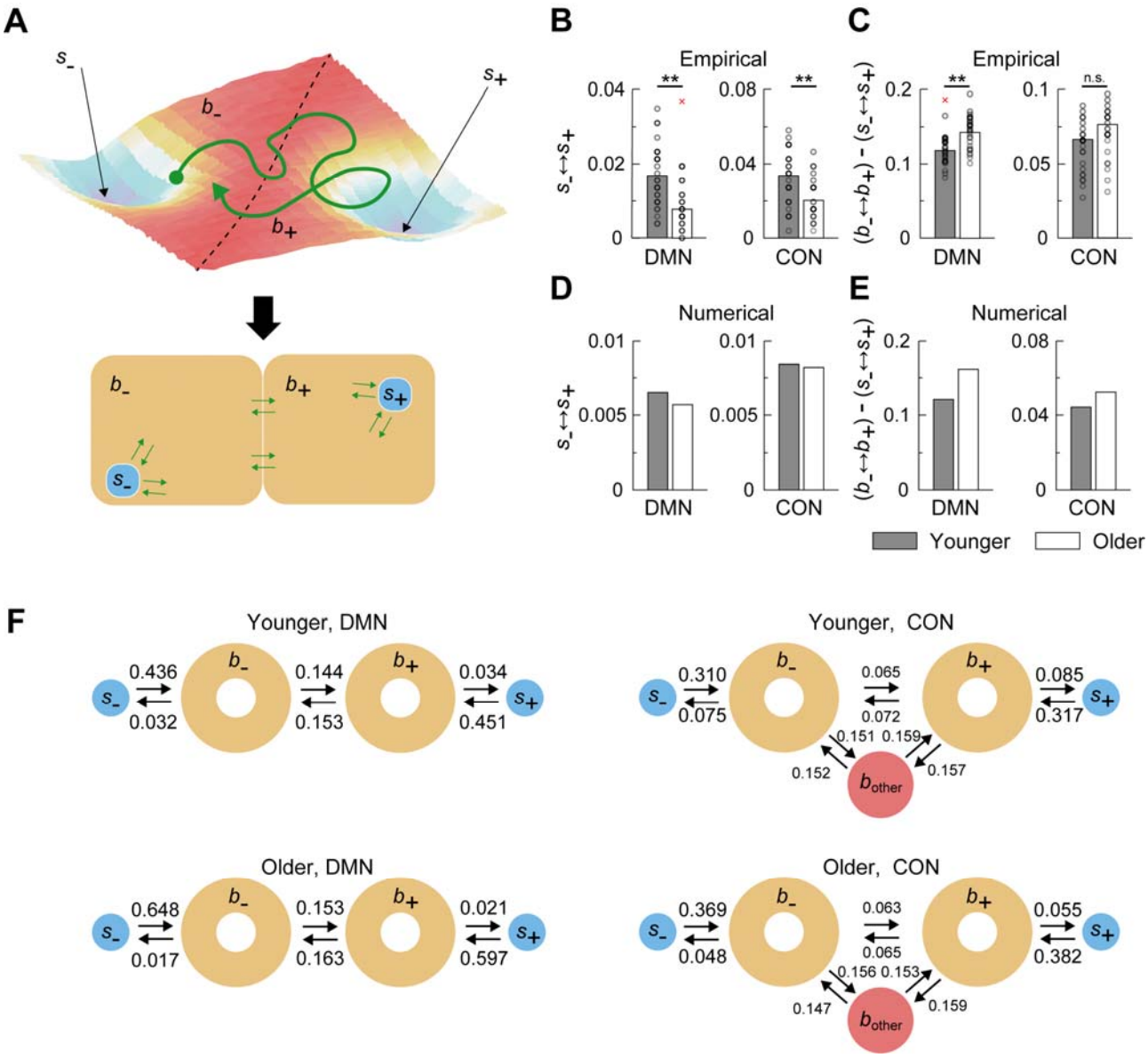

Figure 6. Transition rates on the energy landscape of the DMN and CON. (A) Schematic showing the procedure to categorize the $2^{N_{ROI}}$ activity patterns into four groups in the case of the DMN. The figure on the top depicts a hypothetical energy landscape, similar to Fig. 3, and the dynamics of the activity pattern shown by the movement of a ball. The synchronized activity patterns, s_+ and s_-, are local minimums. The dotted line divides the basins of attraction for s_+ and s_-, i.e., b_+ and b_-. We classified the activity patterns into these four groups. Note that s_+ and s_- are composed of a single synchronized activity pattern. The probability flow between activity patterns is depicted in the figure to the bottom. We aggregate the probability flow from activity patterns in b_- to those in b_+, for example, to obtain the probability flow from group b_- to b_+. (B)-(E) Transition rates compared between the younger and older groups. (B) Rate of transitions between s_+ and s_- for the two systems and two participant groups, calculated from the empirical data. (C) Rate of peripheral transitions calculated from the empirical data. (D) Rate of transitions between s_+ and s_- constructed from the

numerically simulated data. (E) Rate of peripheral transitions calculated from the numerically simulated data. In (B)-(E), the bars represent the group-averaged results. In (B) and (C), a circle represents a participant. A cross represents an outlier. (F) Conditional transition probability (i.e., transition rate divided by the probability that the group of the activity patterns in question is visited) between each possible pair of s_+, s_-, b_+, b_-, and b_{other} in the DMN and CON for the two age groups. See *Supporting Information* for the results separately obtained for the right and left DMNs. $^{**}P_{Bonferroni} < 0.01$, in two-sample *t*-tests ($N_{younger} = N_{older} = 28$ before excluding outliers). Note that the inclusion of the outliers did not influence the statistical significance reported in the main text (main effects of Age: (B) $F_{1,54} = 25.1$, $P < 10^{-5}$, $\eta^2 = 0.34$, (C) $F_{1,54} = 18.4$, $P < 10^{-4}$, $\eta^2 = 0.06$ in two-way factorial Age×System ANOVAs).

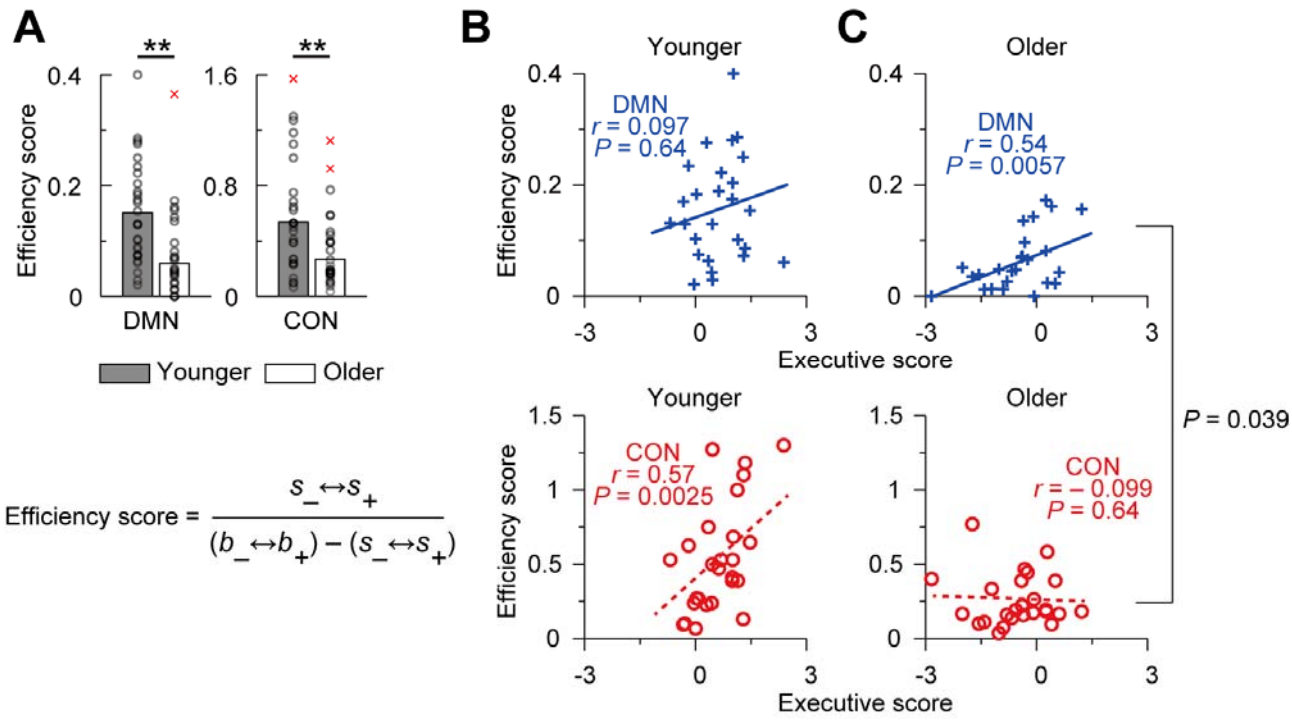

Figure 7. (A) Efficiency score, which measures the ease of transitions between the synchronized activity patterns, compared between the two age groups for the DMN and CON. The bars represent average values excluding the outliers shown by the crosses. A circle and cross represent a (non-outlier) participant and an outlier, respectively. The efficiency scores from one younger adult and two older adults were identified as outliers for the CON, and the efficiency score from one additional older adult was identified as an outlier for the DMN. $^{**}P_{\text{Bonferroni}} < 0.01$ in post-hoc two-sample *t*-tests. The inclusion of the outliers marginally influenced the significance of the age-by-system interaction ($F_{1,54} = 3.92$, $P = 0.053$ in a two-way factorial Age×System ANOVA) but did not influence the main effect of Age ($F_{1,54} = 14.4$, $P < 10^{-3}$, $\eta^2 = 0.08$). Panels (B) and (C) show the relationship between the efficiency score and the executive score. (B) Younger group. (C) Older group. A symbol represents a participant. The Pearson's correlation coefficient, denoted by *r*, was calculated for each age group. The linear regression is shown for the DMN and CON by the solid and dotted lines, respectively. A significant difference was found in the correlation coefficient (*r*) between the DMN and CON in the older group ($t = 2.2$, $P = 0.039$, $r = 0.43$, $N_{\text{older}} = 25$), whereas no significant difference was found in the younger group ($t = 1.74$, $P = 0.096$, $N_{\text{younger}} = 26$). See *Supporting Information* for the results separately obtained for the right and left DMNs.

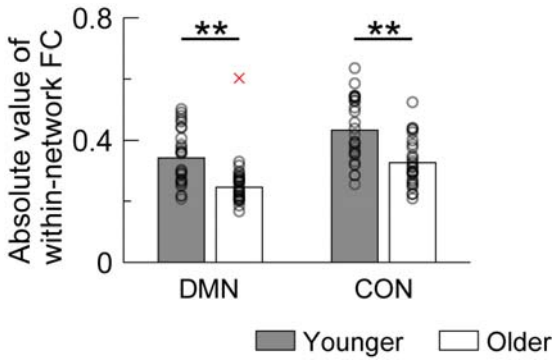

Figure 8. Average functional connectivity compared between the younger and older groups. The circles and the cross represent the averages of the absolute value of the functional connectivity over all ROI pairs in a brain system (i.e., DMN or CON) for (non-outlier) individuals and the outlier, respectively. The bars represent the group averages calculated without the outlier. ** $P_{\text{Bonferroni}} < 10^{-2}$ in post-hoc two-sample *t*-tests. The inclusion of the outlier did not influence the statistical significance of the results (main effect of Age: $F_{1,54} = 23.6$, $P < 10^{-4}$, $\eta^2 = 0.54$, age-by-system interaction: $F_{1,54} = 0.28$, $P = 0.60$ in a two-way factorial ANOVA, [Age: younger/older] × [System: DMN/CON]).

Table 1. Demographic data.

	Younger	Older
Age (mean ± std)	22.61±2.96	70.96±7.51
IQ*		
Performance IQ (mean ± std)	112.71±11.04	111.93±15.43
Verbal IQ (mean ± std)	109.61±12.35	111.16±9.80
Full IQ (mean ± std)	113.04±11.50	111.86±11.87
Female/male	14/14	14/14
Executive score** (mean ± std)	0.55±0.77	-0.53±0.92

* IQ was evaluated by the Wechsler Abbreviated Scale of Intelligence (WASI) (Wechsler, 1999); **, Executive score was determined by the Delis-Kaplan Executive Function System (Delis et al., 2001, 2004).

Table 2. Accuracy of the fitting by the pairwise MEM. Four ROIs in the DMN in the medial part of the brain were shared by the right and left DMNs.

	right DMN	left DMN	whole DMN	whole CON
N_{ROI}	8	8	12	7
Younger	0.930	0.911	0.659	0.973
Older	0.866	0.839	0.467	0.971